A Search for Small-Scale Clumpiness in Dense Cores of Molecular Clouds

L. E. Pirogov[1,*] and I. I. Zinchenko[1]

[1] *Institute of Applied Physics Russian Academy of Sciences*

We have analyzed HCN(1–0) and CS(2–1) line profiles obtained with high signal-to-noise ratios toward distinct positions in three selected objects in order to search for small-scale structure in molecular cloud cores associated with regions of high-mass star formation. In some cases, ripples were detected in the line profiles, which could be due to the presence of a large number of unresolved small clumps in the telescope beam. The number of clumps for regions with linear scales of $\sim 0.2-0.5$ pc is determined using an analytical model and detailed calculations for a clumpy cloud model; this number varies in the range: $\sim 2\times10^4-3\times10^5$, depending on the source. The clump densities range from $\sim 3\times10^5-10^6$ cm^{-3}, and the sizes and volume filling factors of the clumps are $\sim (1-3)\times10^{-3}$ pc and $\sim 0.03-0.12$. The clumps are surrounded by inter-clump gas with densities not lower than $\sim (2-7)\times10^4$ cm-3. The internal thermal energy of the gas in the model clumps is much higher than their gravitational energy. Their mean lifetimes can depend on the inter-clump collisional rates, and vary in the range $\sim 10^4-10^5$ yr. These structures are probably connected with density fluctuations due to turbulence in high-mass star-forming regions.

Key words: interstellar medium, molecular clouds, interstellar molecules, radio lines.

1. INTRODUCTION

The problem of why star formation results in the formation of stars in clusters in some cases and in the appearance of isolated stars in others remains unsolved. It is known that stellar clusters in which high-mass stars are born are associated with higher mass, more turbulent cores of molecular clouds than those in which isolated stars are born. Regions

* Electronic address: pirogov@appl.sci-nnov.ru

of molecular emission associated with such cores probably do not fill the telescope beam completely; instead, they may have an inhomogeneous, clumpy structure that is unresolved in the observations (see, e.g., [1]). There are many indirect pieces of evidence suggesting the existence of small-scale (unresolved) inhomogeneities in the dense cores of interstellar molecular clouds that are birthplaces of high-mass stars and stellar clusters. In particular, a clumpy structure for the molecular emission in objects associated with H II regions and H_2O masers follows from the ratios of the observed peak intensities and widths of lines with different optical depths (see, e.g., [2, 3]); this is confirmed by modeling of line profiles for various rotational transitions of the CS molecule in models with small clumps [4]. The absence of appreciable density variations in giant molecular clouds, where the gas column densities vary by more than an order of magnitude [5], could also be due to the existence of small-scale density inhomogeneities. The masses of the cores derived from calculations of molecular excitation often prove to be higher than the virial masses or masses calculated from observational data on optically thin dust emission, likewise suggesting a clumpy structure for the molecular emission regions (see, e.g., [6]). The detection of extended regions of emission in atomic carbon lines toward a number of high-mass star-forming regions [7] may also testify to the inhomogeneous structure of these regions, where more rarefied photon-dominated regions, where the effects of ultraviolet radiation are important, can apparently coexist with high-density gas.

Important evidence for small-scale clumpiness in high-mass star-forming regions is provided by observations of anomalies in the hyperfine structure of the $J = 1 - 0$ HCN line, manifest as a low relative intensity of the $F = 1 - 1$ component compared to the optically thin case. This is due to the overlap of local profiles of components in higher lying transitions, and depends on the degree of broadening of the local profiles. These anomalies arise in gas with kinetic temperatures ≥ 20 K, and should vanish when the widths of the local profiles become close to that of the observed HCN(1–0) profiles in these objects (≥ 2 km/s). However, if the objects consist of small, randomly moving clumps with densities close to the critical density for the given molecular transition and the line profiles of individual clumps are close to thermal, the observed HCN(1–0) lines will display these anomalies, but have widths corresponding to the velocity dispersion of their relative motions [8].

Estimation of the physical properties of small clumps that are not directly resolved in observations requires detailed calculations of radiative transfer in an inhomogeneous, frag-

mentary medium, with the subsequent computation of line profiles and comparison with the results of observations. This can involve a large number of unknown parameters and be fairly resource-intensive in a full study of the entire space of possible values of these parameters. Martin et al. [9] proposed a simple analytical model in which a cloud was taken to consist of unresolved, randomly moving identical clumps with a small volume filling factor. Using this model, we can use the ratios of the intensities and widths of two lines having different optical depths to derive the relationships between parameters of the clumps. It was pointed out in [10, 11] that, if the volume filling factor of the clumps is low and the number of clumps in the line of sight at a given radial velocity is small, we should expect the appearance of ripples in line profiles. These ripples are due to fluctuations in the number of clumps in the line of sight at various velocities, and can be used to estimate the parameters of the clumps filling the beam.

However, detecting such ripples requires high sensitivity and high spectral resolution. To check the method, the above studies used mainly observational data on the most intense lower transitions of the CO molecule and its isotopic modifications in the dense cores of M17 SW and Orion A. Since these lines are efficient probes of gas with densities of $\sim 10^3$ cm^{-3}, they are most likely tracers of the inter-clump gas, as is inferred by the spatial correlation of the atomic carbon and CO emission (see, e.g., [12]). Searches for small-scale inhomogeneities are probably more fruitfully carried out using lines that trace gas with densities one to two orders of magnitude higher than the low CO transitions, such as CS(2–1) or HCN(1–0).

In this paper, we present measurements of CS(2–1) and HCN(1–0) lines, as well as isotopic modifications of these lines, toward selected positions in three dense molecular-cloud cores associated with highmass star-forming regions and possibly possessing an inhomogeneous, clumpy structure. We used the analytical method of [9, 11] and compared the observational data with the results of detailed calculations for a simple model of a cloud with small clumps. Our analysis has enabled us to estimate the physical properties of small, spatially unresolved clumps in the framework of the models considered.

2. RESULTS OF THE OBSERVATIONS

To confirm the existence of small-scale clumpiness of the dense gas in high-mass star-forming regions, we observed three dense cores associated with high-mass star-forming re-

gions on the 20-m radio telescope in Onsala (Sweden) in 1999. We chose for these observations the objects S140, S199 (IC1848A, AFGL 4029), and S235 (G173.72+2.70), which display anomalies in the hyperfine structure of the $J = 1 - 0$ HCN line, suggesting the existence of small clumps with thermal linewidths [8].

The observations were carried out in the $J = 1 - 0$ line of HCN and $J = 2 - 1$ line of CS at 88.63 and 97.98 GHz, respectively. Some positions were observed in lines of rarer isotopes of these molecules, namely, the $J = 1 - 0$ line of $H^{13}CN$ and $J = 2 - 1$ line of C34S (at 86.34 and 96.41 GHz, respectively). The telescope beamwidths were $45''$ at the HCN(1–0) frequency and $39''$ at the CS frequency. The beam efficiencies at these frequencies were 0.59 and 0.56, respectively. The dependence of this factor on the source elevation was not taken into account; according to later measurements, this could result in an underestimation of the line intensities at low elevations of up to $\sim 30\%$. The single-sideband noise temperature of the system during most of the observing time was $\sim 170 - 350$ K, depending on the weather conditions and source elevation. The observations were carried out toward two positions separated by an angular distance of $1.5'$–$2'$, which exceeded the telescope beamwidth; thus, the distributions of small clumps for these positions could be assumed statistically independent. The signal-to-noise ratios were $\sim 30 - 250$, and the integration times were 1–11 h, depending on the source and observed line. The list of sources, their coordinates and distances, and the spatial resolution of the observations in the various lines are given in Table 1.

The spectrum analyzer was an autocorrelator with a 20-MHz bandwidth and a frequency resolution of 12.5 kHz; this corresponded to a velocity resolution of ~ 40 m/s at the observed frequencies. However, analysis of the spectra at emission-free reference positions showed that adjacent channels of the autocorrelator were not independent (as was also noted in [11]), which degraded the actual spectral resolution. The correlation coefficient between adjacent channels was ~ 0.6, between channels i and $i + 2$ was $\sim 0.2 - 0.3$, and between channels i and $i + 3$ was close to zero. Accordingly, only one of three successive channels was used in the subsequent analysis; thus, the spectral resolution in velocity was 127 m/s.

Figure 1 shows the spectra obtained. The observed profiles demonstrate no self-absorption effects. In a number of cases, the profiles of themain-isotope lines (HCN, CS) obtained with high signal-to-noise ratio display a small asymmetry, which is noticeable during a comparison with the centers of the lines of rarer isotopes. High-velocity wings due to the presence of large-scalemotions in the sources are also present. In S235, the HCN and CS profiles have

more than one component with similar intensities and linewidths.

3. ANALYSIS OF PARAMETERS OF THE OBSERVED LINE PROFILES USING AN ANALYTICAL MODEL

Martin et al. [9] derived an analytical expression for the profile of a line emitted by a cloud consisting of identical clumps moving randomly in space. Assuming that the excitation temperature of the line (Tex) is identical in all the clumps and neglecting the contribution from the microwave background, the radiation temperature of the line is described by the expression:

$$T_{\rm R}(v) = T_{\rm EX}(1 - e^{-\tau_{\rm eff}(v)}) \ . \tag{1}$$

The effective optical depth of a cloud ($\tau_{\rm eff}$) when the velocity dispersion of the clumps (σ) is much greater than that of the gas inside the clumps (v_0) can be written

$$\tau_{\rm eff}(v) = N_c A(\tau_0) \exp(-\pi v^2/\sigma^2) \ , \tag{2}$$

where $A(\tau_0)$ is an integral function that depends on the optical-depth distribution and geometry of the clump, and τ_0 is the maximum optical depth of the clump. When $\tau_0 \ll 1$, we have $A(\tau_0) \simeq \tau_0$. The quantity N_c is the number of clumps in a column with cross-sectional area r_0^2 (r_0 is the clump radius) whose velocities are within v0 of the line center:

$$N_c = K N_{\rm tot} \frac{r_0^2}{B} \frac{v_0}{\sigma} \ , \tag{3}$$

where B is the area of the telescope beam and $N_{\rm tot}$ is the number of clumps in the beam. The factor K depends on the optical-depth distribution in an individual clump. Martin et al. [9] and Tauber [11] assumed a Gaussian dependence for the optical depth on the impact parameter, in which case $K = 1$. In the case of opaque disks, when the optical depth does not depend on the impact parameter, $K = \pi$.

Martin et al. [9] used ratios of the peak intensities and widths of two lines (lower transitions of CO and ^{1}3CO) to find relationships between physical parameters of the clumps in the dense core M17 SW. Tauber [11] proposed an analytical method for determining the clump parameters based on this idea. In addition to the ratios of the peak intensities and widths of two lines, a new parameter was introduced (assuming that $N_c \lesssim 10$):

$$\frac{\Delta T_{\rm R}}{T_{\rm R}} = \frac{\tau_{\rm eff}}{(e^{\tau_{\rm eff}}-1)\sqrt{N_c \frac{B}{{r_0}^2}}} = \frac{\tau_{\rm eff}}{(e^{\tau_{\rm eff}}-1)\sqrt{N_{\rm tot}\frac{v_0}{\sigma}}} \ , \qquad (4)$$

where $\Delta T_{\rm R}$ is the standard deviation for fluctuations of the radiation temperature in some range near the line center relative to a certain expected value; these deviations are related to fluctuations in the number of clumps in the line of sight moving with various velocities. The more rugged and less smooth the line profile, the greater the ratio $\Delta T_{\rm R}/T_{\rm R}$; henceforth, we will call this ratio the "jaggedness" of the line profile, in contrast to the term "smoothness" used in [11].

The values of $T_{\rm R}$, $\Delta T_{\rm R}$ and the widths for two lines with different optical depths can be determined from observations. If one of the lines is optically thin, we can calculate the value of $\tau_{\rm eff}$ for an optically thick line from the linewidth ratio. Knowing the jaggedness and effective optical depth of the line, we can calculate $N_{\rm tot}\frac{v_0}{\sigma}$ using (4). Assuming that the velocity dispersion in the clumps is determined by the thermal gas motions and knowing the kinetic temperature, we can estimate the ratio $\frac{v_0}{\sigma}$ and the number of clumps in the telescope beam. If the jaggednesses and linewidth ratios for two lines with different optical depths are known, we can calculate N_c and τ_0 for one of the lines and estimate the size of a single clump r_0.

Martin et al. [9] and Tauber [11] also used an expression for the ratio of the peak intensities of two lines: $T_{\rm R}^1/T_{\rm R}^2 = (1-\exp(-\tau_{\rm eff}^1))/(1-\exp(-\tau_{\rm eff}^2))$, which is applicable for lines in LTE (e.g., for lower transitions of CO and ^{13}CO). However, it is not appropriate to use this relation for lines of HCN, CS, and their isotopes, for which the distribution of population densities over the rotational levels is appreciably nonequilibrium for the densities and column densities typical of the dense cores of interstellar clouds.

As Tauber [11] pointed out, $\Delta T_{\rm R}$ can be estimated by fitting and subtracting a Gaussian function, a function of the type (1), or triplets with a fixed separation between their components (in the case of HCN); fitting polynomial functions to separate segments of the line profile, with subsequent subtraction; or filtration of the lowest harmonics of the Fourier spectrum, which correspond to the main line profile. After applying these methods, the residual spectrum should be noise-like, possibly with different dispersions within and outside the line. Since the contribution of the emission of a set of small clumps is statistically independent from the atmospheric and instrumental noise in the spectra, we can calculate the standard

deviation for the residual noise: $\Delta T_{\rm R} = \sqrt{\Delta T_{\rm L}^2 - \Delta T_{\rm N}^2}$, where $\Delta T_{\rm L}$ is the standard deviation for temperature fluctuations near the line peak, and $\Delta T_{\rm N}$ is the standard deviation for fluctuations outside the line. In his analysis of line parameters for the spectrum of Orion A, Tauber [11] fit and subtracted a function of the form (1); however, the similarity of the asymmetry in the line profiles obtained toward different positions of the Orion A cloud led him to suspect that there was a spatial correlation of the residual fluctuations, which could be due to systematic motions. This contradicted the idea that the fluctuations related to the small-scale clumpiness were statistically independent, and prevented Tauber [11] from estimating the jaggedness of the profiles. No other methods for estimating $\Delta T_{\rm R}$ were applied in [11].

In the calculations of $\Delta T_{\rm L}$, the three methods mentioned above were applied to all the derived pro- files. If no excess of $\Delta T_{\rm L}$ above $\Delta T_{\rm N}$ was found in at least one of them, it was further assumed that there were no residual fluctuations related to clumpiness in this profile. When calculating $\Delta T_{\rm L}$ by fitting and subtracting polynomials, the bandwidth near the line peak (2–3 km/s) and the order of the fitted polynomial (second to fourth) were varied. The optimal cutoff boundary was chosen for rejecting the lowest Fourier harmonics. Though the main order of the Fourier harmonics corresponding to the observed lines with widths of ≥ 2 km/s is concentrated at reciprocal velocities ≤ 0.5 (km/s)$^{-1}$, the presence of even a small asymmetry in the line profiles of the main isotopes (possibly due to systematic motions in the dense gas) can result in the appearance of features in the power spectra in a broader band than the range corresponding to the effective Gaussian profile, as can be seen from Fig. 2 in the case of S140(0,0). We modeled the emission of a multilayer medium in order to study the effect of systematic line-of-sight motions on the profile of a single line or several nearby lines with optical depths ≥ 1; each of layers had its own lineof-sight velocity and excitation temperature, in accordance with specified power laws. We were able to achieve profile asymmetries similar to those observed by varying the velocity at the boundary and the exponent in the radial dependence of the velocity, as well as the optical depth of an individual layer. Analysis of the power spectra for lines with widths ≥ 2 km/s and with the addition of noise similar to the measurement noise showed that, in Gaussian-like spectra, features associated with systematic motions fall to the noise level on scales $V^{-1} \leq 0.7$ (км/с)$^{-1}$. Therefore, the cutoff boundary for rejecting Fourier harmonics was set to 0.7 (км/с)$^{-1}$ (for the HCN(1–0) profiles in S235, 0.9 (км/с)$^{-1}$). This slightly

underestimates $\Delta T_{\rm L}$, whereas fitting smooth functions to the line profiles or profile segments may yield overestimates. We adopted the standard deviation of the temperature fluctuations in the channels after subtracting the baseline outside the spectral line as $\Delta T_{\rm N}$.

The peak intensities, linewidths, and effective optical depths are listed in Table 2. The values of $T_{\rm R}$ and ΔV were obtained by fitting Gaussians to the observed line profiles. For the HCN(1–0) and $H^{13}CN$(1–0) profiles, these values refer to the central component $F = 2 - 1$; the relative intensities R_{12} and R_{02} are given for the side components, $F = 1 - 1$ and $F = 0 - 1$. In several cases, we list the widths of the $F = 0 - 1$ component, which were used when calculating $\tau_{\rm eff}$. In the remaining cases, $\tau_{\rm eff}$ was calculated by comparing the linewidths for the main and rarer isotopes. The errors in the line intensities and widths were obtained from the fits.

Figure 2 presents the HCN(1–0) and CS(2–1) line profiles toward some observed positions together with the residual noise obtained after rejecting the lowest Fourier harmonics. For each profile, the power spectrum for small amplitudes of the Fourier harmonics is shown at the right; the cutoff boundary is also indicated.

Fluctuations in the residual noise near a line peak were detected most confidently for the $F = 2-1$ HCN(1–0) component. In two cases, fluctuations of the residual noise were detected in the CS(2–1) profiles. No fluctuations exceeding the noise level outside the line were found in the $C^{34}S$(2–1) and $H^{13}CN$(1–0) profiles; thus, were we able to estimate only the total number of clumps in the telescope beam $N_{\rm tot}$, using themethod described above. Table 3 lists the values of $\Delta T_{\rm N}$ and $\Delta T_{\rm R}$. The errors of $\Delta T_{\rm R}$ probably reach $\sim 10 - 20\%$; they are mainly due to our choice of the interval near the line peak for which they are calculated, as well as to the computational method. The table also lists the kinetic temperatures required to calculate the gas velocity dispersion inside the clumps, together with the values of $N_{\rm tot}$. Since uncertainties in $\Delta T_{\rm R}$ and $\tau_{\rm eff}$ strongly influence $N_{\rm tot}$, probably resulting in errors no less than $\sim 50\%$, we retained only two significant figures in these results.

The estimates of $N_{\rm tot}$ based on the HCN(1–0) and CS(2–1) data toward S140(0,0) differ appreciably; this could be due to inter-clump gas resulting in effective smoothing of the fluctuations in the CS(2–1) profiles. This possibility is confirmed by model calculations (see Section 4). In the remaining cases, the estimates based on $\Delta T_{\rm R}$ for these two lines are consistent with each other within the probable errors. For S199(0,0), the value of $\tau_{\rm eff}$ for both lines was calculated from the ratio of the widths of the $F = 2 - 1$ and $F = 0 - 1$ HCN(1–0)

components. However, the estimate of $N_{\rm tot}$ based on this ratio proved to be considerably lower than the value yielded by themodel calculations (see Section 4). This may suggest that this method has overestimated τ_{rmeff}. Toward both positions in S235, the line profiles contain features that could be due to the presence of an individual dense clump in the line of sight is larger than the telescope beam. Its effect is appreciabe in the HCN(1–0) profile toward position (0,0), and it is especially obvious toward position (0,–2) in the CS(2–1) and HCN(1–0) profiles (Fig. 1). Fitting two Gaussians to the CS(2–1) profile and two triplets to the HCN(1–0) profile toward position (0,–2) enabled us to distinguish two components with similar widths at velocities –17 and –16 km/s. The profiles of the $F = 2 - 1$ HCN(1–0) hyperfine component and the CS(2–1) line toward position (0,0) are smoother, with only a slight asymmetry. The estimates $N_{\rm tot}$ were made for the position (0,0); $\tau_{\rm eff}$ for both lines was calculated from the ratio of the CS and $C^{34}S$ linewidths.

4. RESULTS OF NUMERICAL CALCULATIONS IN THE CLUMPY MODEL

Since no residual fluctuations exceeding the noise level were found in the profiles of the optically thin $C^{34}S$(2–1) and $H^{13}CN$(1–0) lines, we were not able to apply the analytical model (Section 3) to determine the physical properties of individual clumps. Instead, we carried out detailed calculations of the excitation of molecules in a cloud model with small clumps. We applied the model described in [8], which was used earlier to explain features in HCN(1–0) spectra observed in clouds associated with high-mass starforming regions, in the calculations. An analysis of the line profile residual intensity fluctuations had not been conducted earlier. For convenience when comparing with the analytical model and to reduce the number of model parameters, we used a simplified version of the model (Model 1). The cloud was assumed to be spherically symmetric, isothermal, and to consist of small cells. Each cell could either be filled with gas (a clump) or be empty, in accordance to a specified probability, which has the meaning of a volume filling factor. The gas density in all clumps was taken to be identical. It was assumed that the clumps have no internal structure and move relative to each other with random velocities having a Gaussian distribution. The line profile from each individual clump was assumed to be Gaussian and to have thermal width. The molecular excitation was calculated for only one representative clump at the cloud center, with all the remaining clumps considered to be identical to it; this matches the

conditions of the analytical model.

We must adjust the temperature, density, abundance of molecules in a clump, and dispersion of the relative motion of the clumps to obtain model profiles that are similar to the observed profiles. The kinetic temperature of the analyzed sources can be considered to be known (Table 3), and the dispersion of the relative motion of the clumps for lines with moderate optical depth (~ 1) can be estimated from their widths. The density and abundance of molecules can be determined fromthe intensities of the HCN(1–0) hyperfine structure, which also depend on the ratio of the filling factor to the size of a single clump. As an example, Figure 3 shows contours for the intensity of the $F = 2-1$ HCN(1–0) component and the relative intensities of the side $F = 1-1$ and $F = 0-1$ components for a kinetic temperature of 30 K and a velocity dispersion of 1.3 km/s as functions of density and HCN column density. The ratio of the volume filling factor to the relative size of a clump (i.e., the ratio of the clump size to the cloud size) is eight and four, respectively, for the left-hand and right-hand graphs; this can reproduce the observed HCN(1–0) profiles in S140 (0,0) and S199 (0,0), respectively.We can roughly estimate density and HCN column density using the observed intensities for the HCN(1–0) components. Knowing the density and temperature and varying the abundances of the $H^{13}CN$, CS, and $C^{34}S$ molecules, we can readily obtain line profiles for these molecules similar to the observed profiles.

Our calculations yielded parameters of the line profiles that are similar to the observed ones (except for the high-velocity wings and asymmetry), including the values of the residual fluctuations $\Delta T_{\rm R}$ (Table 3). We added synthetic noise with a dispersion equal to the dispersion of the observed noise outside the line to the model profiles. The values of $\Delta T_{\rm R}$ were calculated after rejecting the lowest Fourier harmonics (≤ 0.7 (km/s)$^{-1}$) for a 3-km/s interval symmetric about the line center. Since the spatial and velocity distributions of the clumps (which affect $\Delta T_{\rm R}$) depends on the initial value of the random-number generator, we varied the initial values in the calculations and the results were then averaged. The resulting errors in the size of a single clump, volume filling factor, and $N_{\rm tot}$ can reach 20–40%. The spectral resolution was set equal to that of the observations. The probabilities for collisional transitions between the CS rotational levels were taken from [18]. The probabilities for collisional transitions between HCN hyperfine levels were calculated using the method [19]. A k-fold decrease in the size of a clump and in the volume filling factor together with a k-fold increase in the abundance of molecules in a clump will keep the total column density

and component intensities constant, and reduce the jaggedness of the profiles; therefore, by varying these parameters appropriately, we can change the magnitudes of the residual fluctuations near the line peak, fitting them to the observed values.We modeled the HCN(1–0) and CS(2–1) profiles for both positions in S140 as well as for S199(0,0), where the observed profile shapes are close to Gaussian. We did not model the line profiles in S235 because of their multicomponent structure.

The results of the model calculations are presented in Table 4. The total number of clumps in the telescope beam, volume filling factor (f), and size (d) and density (n) of a single clump were obtained by modeling the HCN(1–0) profiles using Model 1. The HCN relative abundances are 10^{-8}, 4×10^{-9}, and 2.3×10^{-9} for S140(0,0), S140(1.5,0), and S199(0,0), respectively. The values of $N_{\rm tot}$ are consistent with the estimates obtained from the analytical model for both positions in S140. However, the calculations for S199(0,0) yield a higher value. This is probably due to overestimation of the effective optical depth in the HCN line toward this position. It is possible that the difference in the widths of the $F = 0 - 1$ and $F = 2 - 1$ components, which was the basis for the calculations of $\tau_{\rm eff}$ in this source, is not due to the optical depth.

However, the model calculations of the CS(2–1) profiles show that, for the same clump-structure parameters as for HCN(1–0), $\Delta T_{\rm R}$ exceeds the observed values. The largest discrepancy is noted for both positions in S140. As was pointed out in [11], taking into account the inter-clump gas can smooth line-profile fluctuations due to clumpy structure if the inter-clump density is sufficient to contribute significantly to the observed lines. This gas can affect the CS(2–1) profile more appreciably than the HCN(1–0) profile, due to the difference in the critical densities for the excitation of these lines. To bring the model $\Delta T_{\rm R}$ values for the CS(2–1) profiles into agreement with the observed ones, we also performed calculations for a model with inter-clump gas of lower density (Model 2). The calculations were carried out in two stages. In the first, we calculated the excitation of molecules in the inter-clump gas assuming a homogeneous, isothermal cloud without clumps. In the second stage, we calculated the excitation of molecules in clumps, but with the cells, which were empty in Model 1, now considered to be filled with inter-clump gas. By varying the density ($n_{\rm ic}$) and abundance of molecules of the inter-clump gas, we can obtain profiles with a jaggedness corresponding to the observed profiles. In the calculations, the CS abundances in clumps and the inter-clump gas were identical; the temperature of the inter-clump gas was set equal

to either the temperature of the gas in clumps or to 200 K, which is fairly characteristic of photon-dominated regions (see, e.g., [20]). The velocity dispersion in the inter-clump gas was taken to be equal to the velocity dispersion of the clumps, which corresponded to the observed profile width. The minimum values of the inter-clump gas density that resulted in effective smoothing of the CS(2–1) profiles and .TR values in agreement with the observed ones are listed in the sixth column of Table 4. The CS relative abundances in the clumps and inter-clump gas were set to be $1.5 \cdot 10^{-9}$, $4 \cdot 10^{-10}$ and $1.4 \cdot 10^{-9}$ for S140(0,0), S140(1.5,0), and S199(0,0), respectively. However, in order for the inter-clump gas to have no effect on the parameters of the HCN(1–0) profiles, we must assume that the HCN abundance is much lower in this gas than in clumps. This could come about due to different HCN formation rates in photon-dominated regions and in clumps. This problem requires further study.

Figure 4 shows model profiles of the HCN(1–0) and CS(2–1) lines; these correspond to the observed profile in S140(0,0), except for the high-velocity component for HCN(1–0). The CS(2–1) profiles are given for Models 1 and 2.

Knowing the sizes and densities of model clumps, we can readily estimate their masses, which proved to be much lower than the clump masses calculated from the condition of virial equilibrium (Table 4). The condition of pressure equilibrium for the clumps is probably not fulfilled. The ratios of the external and internal pressures for the clumps in the model with inter-clump gas (Model 2) are less than unity (Table 4). In fact, the pressure ratios could be lower than the quoted values (by up to a factor of two), due to the difference between the surface turbulent pressure in the medium in which the denser sphere is embedded and the unperturbed pressure far from this region [21].

5. DISCUSSION

The analysis of the previous section has shown that the studied sources can contain a large number of small, nonequilibrium clumps with densities exceeding the inter-clump density by an order of magnitude. We can approximately estimate the lifetime of an isolated clump in a lower-density medium using the virial theorem. For an isothermal, spherical clump subject to external pressure (with the magnetic-field energy of the clump being negligibe), the virial theorem can be written

$$\frac{1}{2}\frac{d^2I}{dt^2} = 3\,Mc^2 - \alpha\frac{GM^2}{R} - 4\pi R^3\,P_{\rm ext}\ \ , \tag{5}$$

where $I \approx M\,R^2$ is the moment of inertia of the clump, M its mass, R its radius, c the speed of sound, α factor of the order of unity that depends on the density distribution (for a uniform distribution, $\alpha = 0.6$), G the gravitational constant, and $P_{\rm ext}$ the external pressure. This equation is widely used to estimate the parameters of clouds and cloud cores in virial equilibrium ($d^2I/dt^2 = 0$). The time during which a clump with mass M and radius R0 will expand to radius R1 is

$$t = \frac{R_0}{\sqrt{3}\,c}\int\limits_1^{x_1}\frac{x\,dx}{\sqrt{(x-x_e)^2 - (1-x_e)^2 - \frac{2\,P_{\rm ext}}{5\,P_{\rm int}}(x^5-1)}}\ \ , \tag{6}$$

where $x_1 = R_1/R_0$, $x_e = R_e/R_0$, $R_e = \alpha\,G\,M/3c^2$ is the radius for which the internal and gravitational energies are equal, and $P_{\rm int} = 3Mc^2/4\pi\,R_0^3$ is the gas pressure inside a sphere with radius R_0. In [22], a similar approach was applied to the expansion of a nonequilibrium, isothermal sphere (without external pressure) in which the internal energy dominated the gravitational energy. In this case, the sphere expands infinitely, and the time required to double its initial radius ($R_1 = 2R_0$), and, accordingly, decrease its density by a factor of eight, was adopted for its lifetime. The gravitational energy of the considered model clumps is much less than their internal energy (x_e is $7\cdot10^{-4}$, $2\cdot10^{-4}$ и $9\cdot10^{-3}$ for S140(0,0), S140(1.5,0), and S199(0,0), respectively). If we set $P_{\rm ext} = 0$ in (6), and neglect x_e compared to x and unity, the solution is $t = \sqrt{(R_1^2 - R_0^2)/3c^2}$. In this case, the time for the initial radius to double is equal to the time for a sound wave to propagate from the cloud's center to its edge, $t_c = R_0/c$, which is $\sim 1.5\cdot10^3$, $\sim 3.9\cdot10^3$ and $t_c \sim 4.5\cdot10^3$ years for S140(0,0), S140(1.5,0), and S199(0,0), respectively.

When the pressure of the inter-clump gas is taken into account, the unlimited expansion of the sphere is replaced by an oscillation mode, with expansion followed by contraction and vice versa. The amplitude of these oscillations can be found from the radicand in (6), which is real and positive only for values of x between unity and some largest value ($x_{\rm max}$) that depends on the pressure ratio. The clumps will expand until they achieve the maximum radius $R_{\rm max} = R_0\cdot x_{\rm max} > R_{\rm eq}$, where $R_{\rm eq}$ is the clump radius when the pressures come to equilibrium. The internal pressure of the gas at $R_{\rm max}$ becomes lower than the external pressure, resulting in contraction. For pressure ratios ~ 0.1, the time when the sphere

reaches $R_{\max}$ only slightly exceeds t_c (only at $P_{\rm ext}/P_{\rm int} = 10^{-3}$ will it reach $\sim 10\,t_c$). For the considered model clumps, the period of the oscillations is $\sim (1.3 - 2.8)\,t_c$.

Though this analysis is fairly simplistic, Keto et al. [23] and Broderick et al. [24] considered the oscillation mode of a pressure-confined, isolated cloud with internal thermal motions and without magnetic field in detail. They found that the lifetime of the oscillations can be fairly long, comparable to the lifetime of the cloud, and is mainly determined by radiative losses and nonlinear interactions between the oscillation modes. In our model with a large number of identical, spherical clumps moving at random velocities relative to each other, lifetimes of the clumps may be determined by the mean time between collisions, if clumps are destroyed after a collision. This time is L_f/V, where L_f is the mean free path of a clump in the cloud and V is the most probable velocity of the clumps. Supposing that $L_f = (n_f\,d^2)^{-1}$, where n_f is the number density of clumps and V is the velocity dispersion in the inter-clump gas, we find that the mean lifetime of the clumps is $\sim 1.7 \cdot 10^4$ years for both the considered regions in S140 and $\sim 8.4 \cdot 10^4$ years for the region toward S199(0,0).

Such short-lived, nonequilibrium structures are probably fluctuations of density enhancements arising due to turbulence in a region of formation of highmass stars and star clusters. If so, our model with identical, spherical clumps will describe the characteristics of the fluctuations only approximately. A more detailed study of the origin and evolution of small-scale density inhomogeneities in a turbulent medium requires the use of three-dimensional, magnetohydrodynamic models together with radiativetransfer calculations in both lines and continuum. Important information on the gas structure in regions of high-mass star formation can be obtained from future high-sensitivity, high-spectral-resolution observations in lines of molecules with considerably different critical densities. The parameters of the smallscale structure in objects of this class should be provided by direct observations with a spatial resolution of $\lesssim 0.1''$, using new-generation interferometers planned to operate in the next decade (see, e.g., [25]).

6. CONCLUSIONS

We carried out high signal-to-noise observations of the HCN(1–0) and CS(2–1) line profiles toward selected positions in the dense cores of the clouds S140, S199, and S235, with the aim of searching for small-scale structure in molecular cloud cores associated with regions

of formation of high-mass stars. Some positions were also observed in the $C^{34}S(2–1)$ and $H^{13}CN(1–0)$ isotope lines.

In several cases, we found ripples in the line profiles of the main isotopes, which can be interpreted as revealing the presence of a large number of unresolved small clumps in the telescope beam. We have used the analytical model [9, 11] to estimate the total number of small clumps in the telescope beam on scales $\sim 0.2 - 0.5$ pc, which can be $\sim 2 \cdot 10^4 - 3 \cdot 10^5$ depending on the source.

Detailed calculations of the excitation of the HCN and CS lines in a cloud model consisting of a set of small thermal clumps that are randomly distributed and move with random velocities have enabled us to estimate physical properties of clumps toward two positions in the dense core of S140 and in S199(0,0). The densities in the clumps are $\sim 3 \cdot 10^5 - 10^6$ cm^{-3}, and their sizes are $\sim (1–3) \cdot 10^{-3}$ pc. The volume filling factors of the clumps are $\sim 0.03–0.12$. To bring the parameters of the HCN and CS profiles into agreement, we must include an inter-clump gas with a density no lower than $\sim (2 - 7) \cdot 10^4$ см$^{-3}$.

The internal thermal energy of the clump gas far exceeds the gravitational energy; and the condition of pressure equilibrium with the inter-clump gas is likewise not fulfilled. When isolated, such spherical clumps can undergo long-term oscillations. The mean lifetime for a set of clumps can be determined from the mean time between collisions: $\sim 10^4 - 10^5$ years. Such structures probably represent density fluctuatins arising due to turbulence in regions of formation of high-mass stars.

ACKNOWLEDGMENTS

The authors are grateful to the staff of the Onsala Observatory for their help with the observations. Large contribution in data acquisition was done by untimely gone L.E.B. Johansson. This work was supported by the Russian Foundation for Basic Research (project codes 06-02-16317 and 08-02-00628) and the Basic Research Program of the Division of Physical Sciences of the Russian Academy of Sciences on “Extended Objects in the Universe".

---

1. J. Kwan and D. B. Sanders, Astrophys. J. 309, 783 (1986).

2. I. I. Zinchenko, A. V. Lapinov, and L. E. Pirogov, Astron. Zh. 66, 1142 (1989) [Sov. Astronomy 33, 590 (1989)].
3. I. Zinchenko, L. Pirogov, and M. Toriseva, Astron. Astrophys. Suppl. Ser. 133, 337 (1998).
4. M. Juvela, Astron. Astrophys. 329, 659 (1998).
5. E. A. Bergin, R. L. Snell, and P. F. Goldsmith, Astrophys. J. 460, 343 (1996).
6. L. Pirogov, I. Zinchenko, P. Caselli, et al., Astron. Astrophys. 461, 523 (2007).
7. G. J. White and R. Padman, Nature 354, 511 (1991).
8. L. Pirogov, Astron. Astrophys. 348, 600 (1999).
9. H. M. Martin, D. B. Sanders, and R. E. Hills, Mon. Not. R. Astron. Soc. 208, 35 (1984).
10. J. A. Tauber, P. F. Goldsmith, and R. L. Dickman, Astrophys. J. 375, 635 (1991).
11. J. A. Tauber, Astron. Astrophys. 315, 591 (1996).
12. M. Ikeda, T. Oka, K. Tatematsu, et al., Astrophys. J. Suppl. Ser. 139, 467 (2002).
13. M. Fich and L. Blitz, Astrophys. J. 279, 125 (1984).
14. R. L. Snell, Y.-L. Huang, and R. L. Dickman, et al., Astrophys. J. 325, 853 (1988).
15. J. Brand and L. Blitz, Astron. Astrophys. 275, 67 (1993).
16. S. Yu. Malafeev, I. I. Zinchenko, L. E. Pirogov, et al., Pis'ma Astron. Zh. 31, 262 (2005) [Astron. Lett. 31, 239 (2005)].
17. I. Zinchenko, Th. Henning, and K. Schreyer, Astron. Astrophys. Suppl. Ser. 124, 385 (1997).
18. F. Lique, A. Spielfiedel, and J. Cernicharo, Astron. Astrophys. 451, 1125 (2006).
19. D. A. Varshalovich and V. K. Khersonsky, Astrophys. Lett. 18, 167 (1977).
20. D. J. Hollenbach and A. G. G.M. Tielens, Ann. Rev. Astron. Astrophys. 35, 179 (1997).
21. C. F. McKee and E. G. Zweibel, Astrophys. J. 399, 551 (1992).
22. E. Vazquez-Semadeni, J. Kin, M. Shadmehri, and J. Ballesteros-Paredes, Astrophys. J. 618, 344 (2005).
23. E.Keto, A. E. Broderick,C. J. Lada, et al.,Astrophys. J. 652, 1366 (2006).
24. A. E. Broderick, E. Keto, C. J. Lada, et al., Astrophys. J. 671, 1832 (2007).
25. ALMA–The Atacama Large Millimeter/Submillimeter Array, `http://www.alma.info`

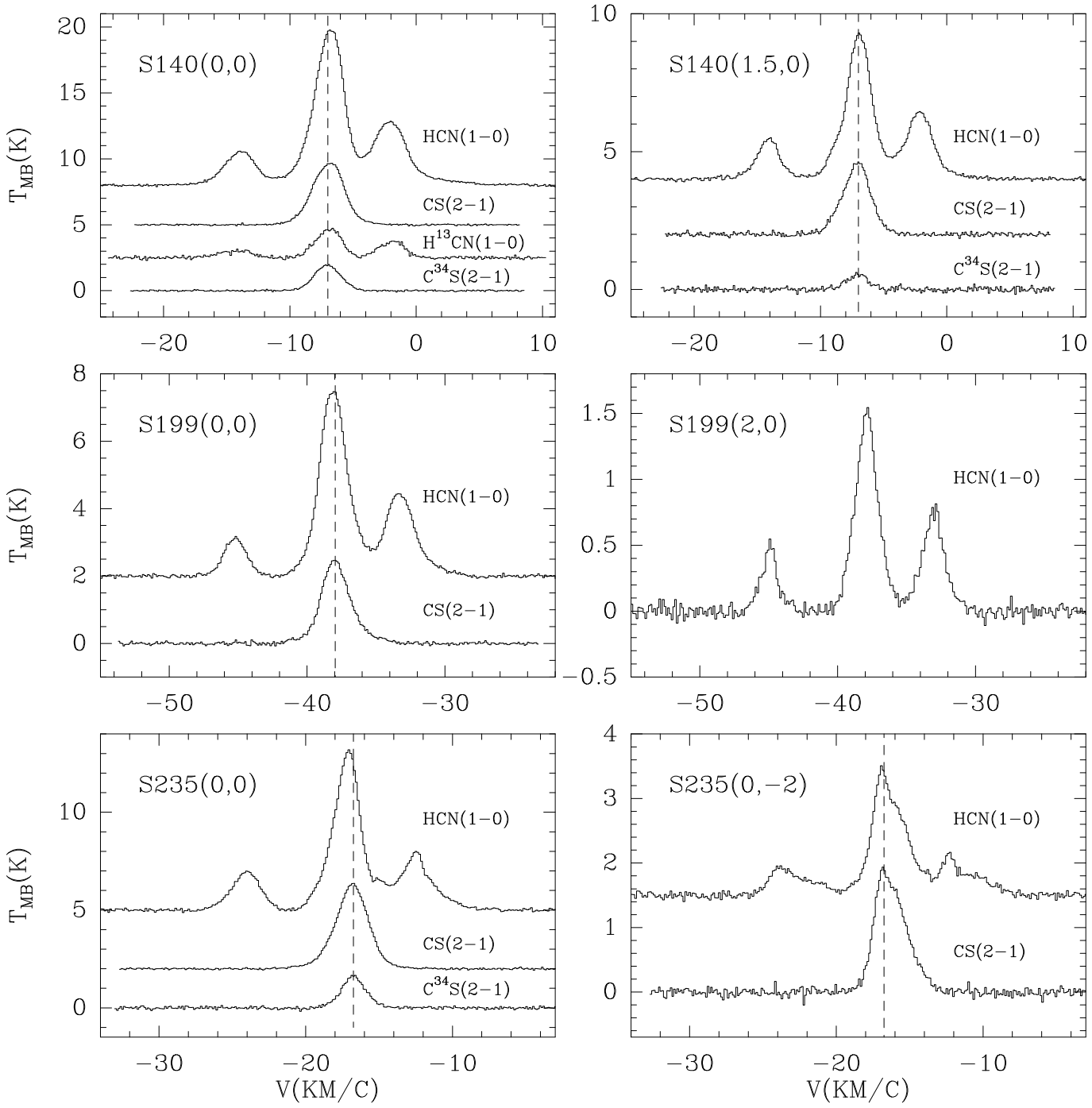

Figure 1. Measured spectra. The dashed line shows the centers of the optically thin $C^{34}S$ lines or CS lines.

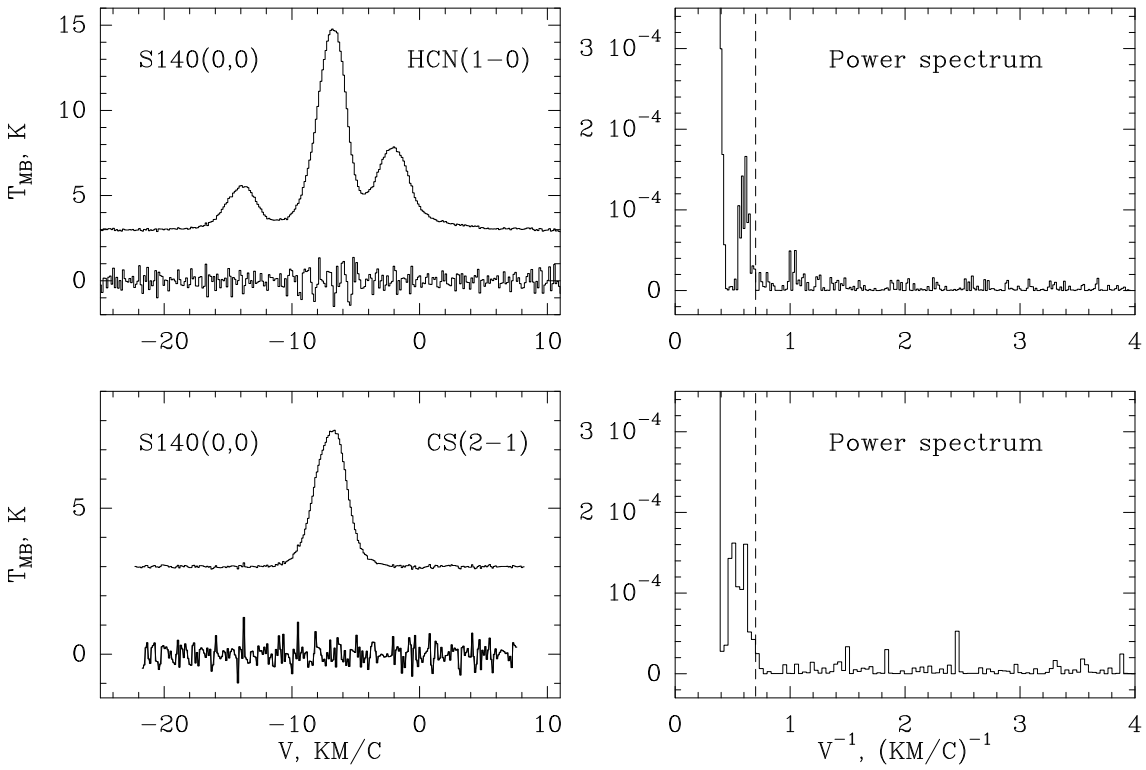

Figure 2. Observed profiles of the HCN(1–0) and CS(2–1) lines together with the residual fluctuations after rejection of the lowest Fourier harmonics. The amplitude of the residual fluctuations is magnified by a factor of ten. The power spectra are shown to the right; the dashed vertical line shows the cutoff boundary.

Table 1. Source list

Source	α(1950) (^{h}) (^{m}) (^{s})	δ(1950) (^{o}) ($'$) ($''$)	D (kpc)	Resolution (pc)
S140	22 17 41.3	63 03 40	0.9 [13]	0.17–0.19
S199	02 57 35.6	60 17 22	2.2 [14]	0.41–0.46
S235	05 37 31.8	35 40 18	2.3 [15]	0.43–0.48

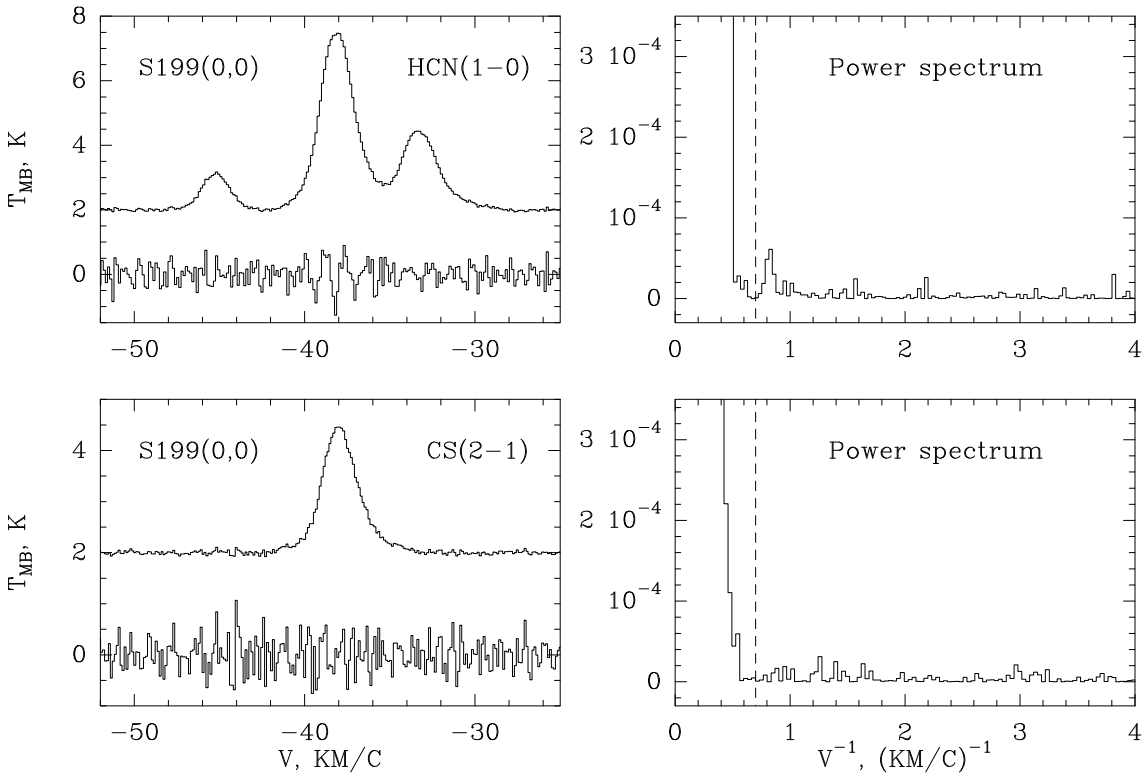

Figure 2. Contd.

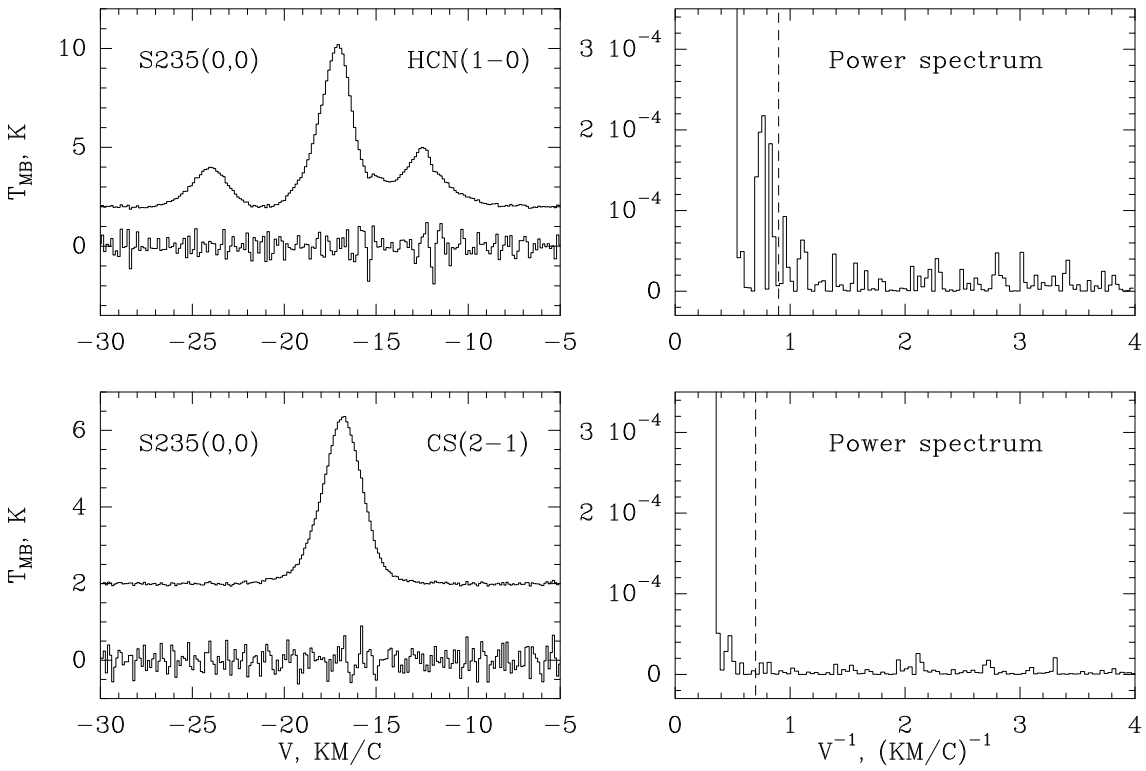

Figure 2. Contd.

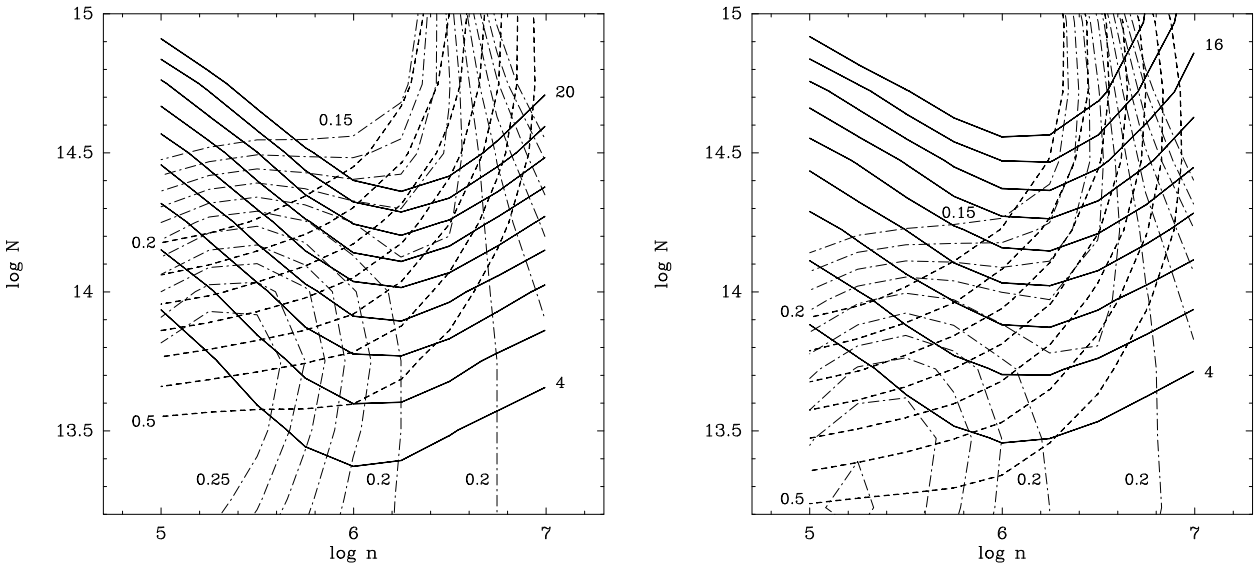

Figure 3. Results of calculations of the HCN(1–0) line excitation in a model with thermal clumps for two ratios of the volume filling factor to the clump size. The contours correspond to the brightness temperatures for the $F = 2 - 1$ component (thick solid curves, step 2 K), the relative intensities of the $F = 1 - 1$ component (dashed curves, step 0.05) and the relative intensities of the $F = 0 - 1$ component (dash-dot curves, step 0.01). The range of variation of the values is indicated in the figure. The physical properties of the model are indicated in the text.

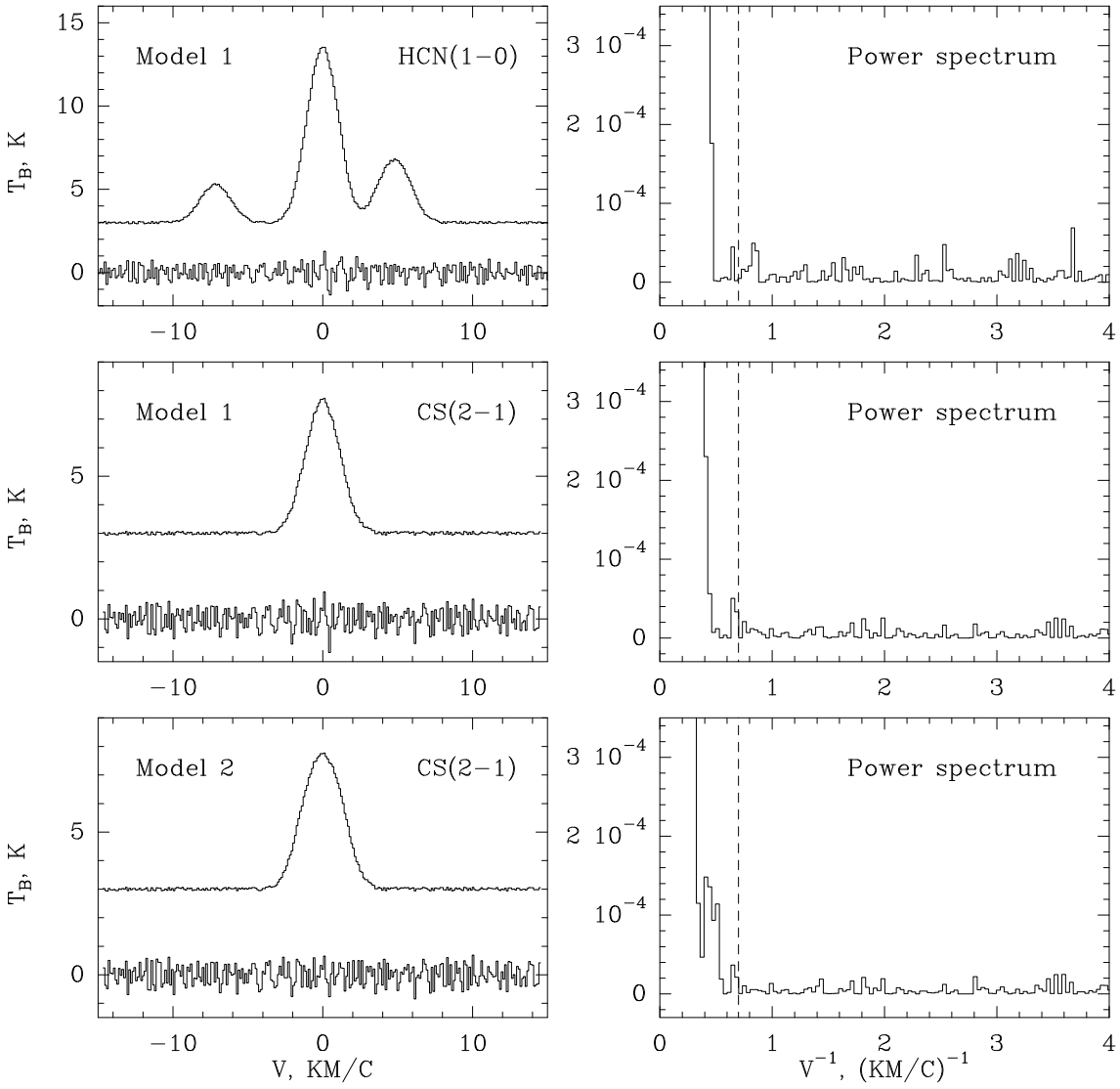

Figure 4. Model profiles of the HCN(1–0) and CS(2–1) lines corresponding to those observed in S140(0,0) and obtained for a clumpy model without (Model 1) and with (Model 2) inter-clump gas. Synthetic noise with dispersion equal to that of the noise observed outside the line range was added to the profiles. The residual noise obtained after filtration of the lowest Fourier harmonics is shown beneath the model profiles, with its amplitude magnified by a factor of ten. The corresponding power spectra for small amplitudes is shown to the right; the dashed vertical line shows the cutoff boundary, 0.7 $(\mathrm{km/s})^{-1}$. The model parameters are given in the text.

Table 2. Parameters of the observed lines

Source	Line	$T_{\rm R}$(K)	R_{12}, R_{02}	ΔV(km/s)	$\tau_{\rm eff}$
S140 (0',0')	HCN(1–0)	10.9(0.1)[1]	0.38, 0.20	2.55(0.01)	0.42(0.03)
	$H^{13}CN$(1–0)	1.09(0.02)	0.57, 0.24	2.37(0.04)	
	CS(2–1)	4.70(0.02)		2.90(0.01)	1.05(0.05)
	$C^{34}S$(2–1)	0.97(0.01)		2.44(0.02)	
S140 (1.5',0')	HCN(1–0)	5.06(0.03)	0.47, 0.28	2.50(0.02)	0.9(0.2)
				2.14(0.05)[2]	
	CS(2–1)	2.52(0.02)		2.61(0.02)	1.6(0.4)
	$C^{34}S$(2–1)	0.27(0.01)		2.0(0.1)	
S199 (0',0')	HCN(1–0)	5.44(0.03)	0.43, 0.20	2.40(0.01)	1.6(0.3)
				1.87(0.06)[2]	
	CS(2–1)	2.4(0.02)		2.45(0.02)	
S199 (2',0')	HCN(1–0)	1.45(0.02)	0.50, 0.31	2.00(0.03)	
S235 (0',0')	HCN(1–0)	~ 8[3]		2.29(0.03)[2]	
	CS(2–1)	4.21(0.02)		2.59(0.01)	1.9(0.1)
	$C^{34}S$(2–1)	0.79(0.01)		1.95(0.03)	
S235 (0',–2')	HCN(1–0)	~ 2[3]			
	CS(2–1)	~ 1.8[3]		~ 2.5[3]	

[1] – After subtracting the high-velocity component.

[2] – Width of the $F = 0 - 1$ component.

[3] – More than one component in the profiles.

Table 3. Residual fluctuations in the line profiles and the total number of clumps in the telescope beam calculated in the analytical model

Source	Line	$\Delta T_{\rm N}$(K)	$\Delta T_{\rm R}(K)$	$T_{\rm KIN}$(K)	$N_{\rm tot}$
S140 (0',0')	HCN(1–0)	0.042	0.055	30 [16]	$\sim 2.6 \cdot 10^5$
	$H^{13}CN$(1–0)	0.037			
	CS(2–1)	0.035	< 0.015		$> 4.2 \cdot 10^5$
	$C^{34}S$(2–1)	0.018			
S140 (1.5',0')	HCN(1–0)	0.035	0.055	39 [16]	$\sim 2.7 \cdot 10^4$
	CS(2–1)	0.051	< 0.02		$> 2.5 \cdot 10^4$
	$C^{34}S$(2–1)	0.035			
S199 (0',0')	HCN(1–0)	0.032	0.053	28 [17]	$\sim 1.7 \cdot 10^4$
	CS(2–1)	0.031	0.016		$\sim 3.9 \cdot 10^4$
S235 (0',0')	HCN(1–0)	0.050	0.056	40 [3]	$\sim 2.3 \cdot 10^4$
	CS(2–1)	0.027	0.025		$\sim 4.0 \cdot 10^4$
	$C^{34}S$(2–1)	0.026			

Table 4. Physical parameters of clumps obtained from model calculations

Source	$N_{\rm tot}$	f	d (pc)	n ($\rm cm^{-3}$)	$n_{\rm ic}$ ($\rm cm^{-3}$)	M ($M_\odot$)	$M_{\rm vir}$ ($M_\odot$)	$P_{\rm ext}/P_{\rm int}$
S140 (0',0')	$\sim 2.8 \cdot 10^5$	$4.2 \cdot 10^{-2}$	$\sim 10^{-3}$	$8.5 \cdot 10^5$	$5 \cdot 10^4$	$\sim 3 \cdot 10^{-5}$	0.062	0.2
S140 (1.5',0')	$\sim 3.6 \cdot 10^4$	$1.2 \cdot 10^{-1}$	$\sim 3 \cdot 10^{-3}$	$3.4 \cdot 10^5$	$7 \cdot 10^4$	$\sim 3 \cdot 10^{-4}$	0.25	0.5
S199 (0',0')	$\sim 1.1 \cdot 10^5$	$2.5 \cdot 10^{-2}$	$\sim 3 \cdot 10^{-3}$	$1.2 \cdot 10^6$	$2 \cdot 10^4$	$\sim 10^{-3}$	0.19	0.06